Reflectance Reduction in a Whiskered SOI Star Coupler

Claudio Castellan, Stefano Tondini, Mattia Mancinelli, Christophe Kopp, and Lorenzo Pavesi, *Senior Member, IEEE*

***Abstract*— In this letter, we evaluate how the background noise is modified within a whiskered-shaped star coupler, optimized to reduce the reflectivity of its internal surfaces to reduce the back-scattered light. This letter is carried out by analyzing the Fabry–Perot interference due to the reflections between the input focal plane of the star coupler and the output facet of the waveguides. By comparing a whiskered star coupler with a standard one, we find a reduction in the star coupler reflectance of more than one order of magnitude. The experimental results are supported by a theoretical model and by numerical simulations.**

***Index Terms*— Nanophotonics, silicon photonics, silicon-on-insulator, optical waveguides, electromagnetic reflection.**

I. Introduction

SILICON-ON-INSULATOR (SOI) photonic devices are particularly sensitive to the presence of unwanted reflections from interfaces, since the reflection coefficient is high due to the large refractive index contrast between silicon and silica [1]. Several strategies have been applied in order to cope with this problem in devices realized on the SOI platform. For example, the shallow etching technique has been introduced for reducing the reflections on the narrow edges between adjacent waveguides in Arrayed Waveguide Gratings (AWGs) [2]–[4]. However, unwanted reflections in SOI devices are not only caused by narrow edges, but also by large Si/SiO_2 interfaces. The edges of a Star Coupler (SC) that are used in AWGs are an example. Another example can be found in the facets at the output of the multimode interference couplers (MMIs). A way to reduce the interface reflectivity is to incorporate lossy waveguides. Lossy waveguides can be realized by using multimode waveguides, that are bent in order to excite the higher order modes and whose width is then adiabatically reduced up to supporting only the first order mode [5]. In this way, the higher order modes are scattered away. Nevertheless, this method requires a large footprint. Another technique proposed to reduce the reflections is the use of subwavelength grating structures, through which the facet power reflectivity is lowered [6]. However, such structures can be often unavailable because of the photolithographic resolution limits. Another possibility is to use inverse tapered waveguides, where the waveguide width (or height) is progressively reduced in order to delocalize the mode, that hence is coupled to the silicon substrate [7]–[9]. Also the performances of this design are related to the lithography resolution, that fixes a minimum width to which the waveguide can be tapered down and which still reflects.

In this letter, we suggest a strategy to decrease the internal reflectance in a SC [10], [11]. Our approach consists in placing on the edges of the SC a series of inversely tapered waveguides that end in structures optimized for minimizing back-reflections. These geometries act as light traps, overcoming the resolution issues affecting the standard inversely tapered waveguides and requiring a small footprint.

II. Experimental Approach

A. Reflectance Decrease by Whiskers

The analyzed structures are based on a 1×21 design, where the output waveguides differ in length. They are produced on a SOI structure with a 220 nm silicon layer height. These SCs can be also considered as the input or output stages of an AWG. In this letter, we are going to compare the behavior of a standard SC (Fig. 1(a)) with that of a SC where the facets are optimized to reduce back-reflections (Fig. 1(b)).[1]

The novelty of our approach consists in placing, perpendicularly to the focal lines of the SC, a series of inversely tapered waveguides that end in a particular geometry acting as *reflection killer*. Henceforth, we will refer to these structures as *whiskers*. In order to maximize the collected power, the whiskers are placed perpendicularly to the focal lines of the SC, and their separation is 160 nm, that is the minimum value allowed by our lithographic process. The waveguide width is adiabatically reduced from 2 μm up to 130 nm in a 30 μm length taper. Accordingly to finite element method (FEM) simulations, the back-reflections in the taper are minimized.

[1]For both the geometries, the input waveguide width is 2 μm and the SC radius is 30.27 μm. The separation between the waveguides at the SC output is 160 nm. Their width is 800 nm, this is adiabatically reduced to 480 nm in the bends to avoid the excitation of higher order modes. Moreover, the SC geometry has been chosen to couple 99% of the light diffracted by the input waveguide to the 21 output waveguides.

Manuscript received March 2, 2016; revised May 13, 2016; accepted May 25, 2016. Date of publication June 2, 2016; date of current version June 30, 2016. This work was supported by the European Commission grant *IRIS*, under Project 619194 FP7-ICT.

C. Castellan, M. Mancinelli, and L. Pavesi are with the Nanoscience Laboratory, Department of Physics, University of Trento, Trento 38123, Italy (e-mail: claudio.castellan@unitn.it; mattia.mancinelli@unitn.i; lorenzo.pavesi@unitn.it).

S. Tondini is with the Nanoscience Laboratory, Department of Physics, University of Trento, Trento 38123, Italy, and also with the Department of Physics, Informatics and Mathematics, University of Modena and Reggio Emilia, Modena 41125, Italy (e-mail: stefano.tondini@unitn.it).

C. Kopp is with the Laboratoire d'électronique des technologies de l'information, Commissariat à l'Energie Atomique et aux Energies Alternatives, Minatec, Grenoble 38054, France (e-mail: christophe.kopp@cea.fr).

Color versions of one or more of the figures in this letter are available online at http://ieeexplore.ieee.org.

Digital Object Identifier 10.1109/LPT.2016.2574364

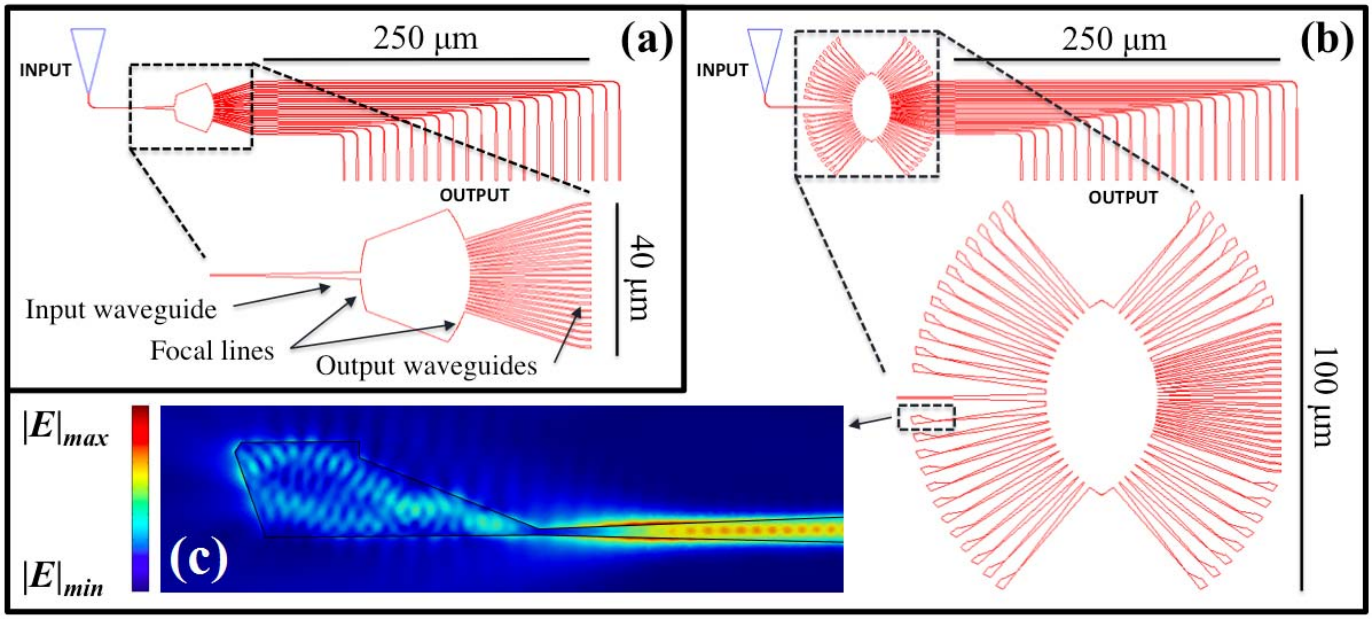

Fig. 1. (a) Standard SC with 1 input waveguide and 21 output waveguides. (b) Whiskered SC with 1 input waveguide and 21 output waveguides. (c) FEM simulation of the electric field profile propagating through the reflection killer geometry.

The geometric parameters of the reflection killer have been optimized in order to create a light trapping system, where the light undergoes to multiple reflections. At each reflection part of the light is scattered away, and so back-reflections are minimized. The performances of the reflection killer have been verified by FEM simulations as it can be seen in Fig. 1(c).

Since the back-reflections of an inverse taper are strictly correlated to the photolithographic resolution, we want to point out that this approach is particularly useful in the case of inverse tapers produced by low resolution processes. In fact, in low resolution processes the waveguide width cannot be reduced to values suitable for delocalizing the mode and suppressing the mode by leakage to the silicon substrate. Therefore, the inverse tapering technique does not work. However, our reflection killer acts as a light trap and is based on multiple scattering from the surfaces. This working principle applies even if the waveguide width at the input of the reflection killer is large.

In order to evaluate the improvements of the whiskered design with respect to the standard one, we analyze the Fabry-Perot (FP) interference in the transmitted signal for both the structures [12], [13]. A tunable laser source in the range between 1520 and 1580 nm is used to couple the light into the devices via a grating coupler. The grating coupler allows for coupling only TE modes, while the waveguides of the system are optimized for supporting only the first order mode. The output light is collected from the waveguide output facet with a tapered optical fiber connected to a germanium detector.

B. Fabry-Perot Interference

In Fig. 2(a) we superimpose the output spectra of the analyzed devices. The spectra show FP oscillations with larger amplitude for the standard design. This is pointed out also by the Fast Fourier Transform (FFT) of the spectra, which peaks at the same frequency but differs in magnitude (Fig. 2(b)).

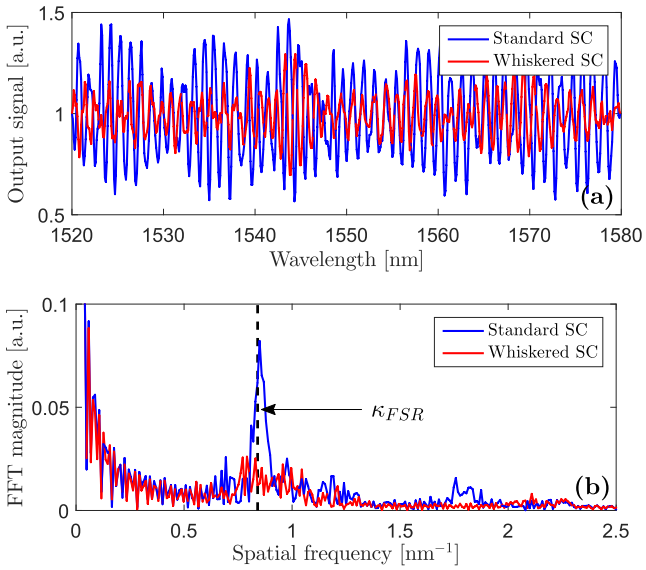

Fig. 2. (a) Experimental output spectrum for the central waveguide of the standard SC (blue) and of the whiskered SC (red). (b) FFT of the measured spectra. The dashed line represents the spatial frequency predicted by FP theory.

One of the reflecting surfaces causing the FP oscillation is the ending facet of the output waveguide. The second reflection surface is the input focal plane of the SC. In fact, by analyzing different devices with longer input waveguides, the main oscillation frequency does not change, indicating that the input waveguide is not part of the FP cavity. Therefore, the light coming from the input waveguide is diffracted into the SC, and it is coupled within the 21 output waveguides. At the output facet, where the silicon waveguides end in air, light is partially reflected back following the Fresnel law [14]. Back-reflected light is again diffracted within the free propagation region, and the facet of the SC in turn reflects it, acting as

a parabolic mirror. Due to the symmetry of the system, for the central waveguide, the light is expected to be reflected toward the same waveguide where it comes from. For the other waveguides, this becomes an approximation that becomes worse as we move away from the center. From FP theory [14], when the light impinges perpendicularly on a mirror, the free spectral range in the wavelength reciprocal space is:

$$\kappa_{FSR} = \frac{1}{\lambda_{FSR}} \simeq \frac{2Ln_g}{\lambda_0^2}, \tag{1}$$

where λ_{FSR} is the FP free spectral range in wavelength space, L is the distance between the mirrors, λ_0 is the wavelength at which constructive interference occurs and n_g is the group index of the mode. We estimate n_g as a weighted average of both the SC and the output waveguide group indices, calculated by mode analysis simulations.

The dashed line in Fig. 2(b) represents the spatial frequency predicted by (1) for a wavelength of 1550 nm. The carrier spatial frequency in the FFT matches the one predicted by the FP theory. The broadening of the experimental FFT peak is related to the fact that κ_{FSR} is a function of $n_g(\lambda)$. Furthermore, part of the light reflected by the SC can be coupled into a different waveguide than the one it is coming from, due to facet roughness. Thus, within a waveguide it is possible to find signal components with FP spatial frequencies corresponding to the adjacent waveguides. This last effect is the reason of the beatings observed in the spectrum of Fig. 2(a).

III. Theoretical Model

To evaluate the reflectance reduction induced by the presence of whiskers, we suggest a model to fit the experimental spectrum. From the transfer matrix theory [14] we derive that, in the case of a FP cavity, the ratio between the electric field E_j transmitted by the j-th waveguide and the incident one E_0 is given by:

$$t_j = \frac{E_j}{E_0} = \frac{\sqrt{(1-R_f)(1-R_s)}\exp(-i\phi-\alpha)}{1-\sqrt{R_f R_s}\exp(-i2\phi-2\alpha)}, \tag{2}$$

where R_f and R_s represent the reflectances of the output facet and the SC facet. The factor $\phi = nkL$ is the phase that the light acquires during the facet to facet path, where n is the cavity refractive index, k the wave number and L the cavity length. The factor α accounts for the cavity losses. In our case $\alpha = \alpha_P L + \alpha_{WG}$, where α_P are propagation losses and α_{WG} is a factor that takes into account the presence of the input waveguide losses.

The model considers also the interaction between reflections from the adjacent waveguides. In particular we estimate the total transmission coefficient τ_k for the k-th waveguide as:

$$\tau_k = \sum_{j=1}^{N} A_{jk} t_j, \quad A_{jk} = \exp\left(-\frac{(j-k)^2}{2\sigma^2}\right). \tag{3}$$

Here we introduced the factor σ, that accounts for the fraction of the adjacent signal that goes into the j-th waveguide. The sum runs over all the $N = 21$ output waveguides. We remark that $|\tau_k|^2$ represents the output spectrum of the k-th waveguide.

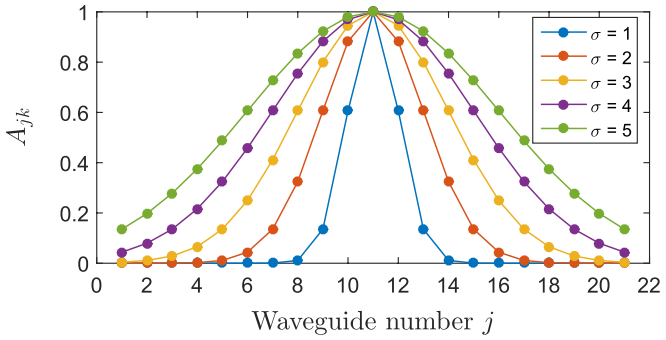

Fig. 3. Behavior of the term A_{jk} appearing within the sum of (3) for the central waveguide $k = 11$ and for different values of σ.

The behavior of the term A_{jk} is reported in Fig. 3 for the waveguide $k = 11$. In particular, the behavior of such a term is shown for different possible values of σ. This term accounts for the amount of field coming from the adjacent waveguides (labeled by j) that goes in the k-th waveguide.

IV. Reflectance Evaluation

Once that all the parameters in (2) and (3) are estimated, we can use (3) to fit the experimental data. The reflectance of the output facet R_f has been estimated by means of a FEM analysis of a SOI waveguide ending in air. The phase factor ϕ also comes from a FEM simulation. The propagation losses have been experimentally evaluated, while α_{WG} is analytically calculated by diffraction integral [15]. What is still missing is the SC reflectance R_s and the value of σ.

A. Model Optimization Using the Standard Star Coupler

For the standard SC, we find the R_s value by simulating a SOI slab ending in silica. Therefore, by evaluating τ_k for the output waveguides, we choose the value of σ that provides the best fit of the experimental spectra.

Fig. 4(a) shows the FFT of the central output waveguide spectrum of three, nominally identical, standard devices. On the plots both the experimental and simulation results are reported. We reach the best agreement between the curves with $\sigma = 1.02$. The experimental curves show also a background noise, which can be ascribed to geometry edges acting as scattering points.

A key parameter for comparing simulation and experiment is the maximum value assumed by the FFT of the optical signal at the FP frequency. In Fig. 4(b) we report the values obtained from experiment and simulation. We focus on the inner waveguides, from the 8-th to the 14-th. In fact, the FP signal in the more external waveguides is much smaller, due to the lower intensity diffracted by the input waveguide at the periphery of the SC.

B. Reflectance Evaluation in a Whiskered Star Coupler

For the whiskered SC, R_s and σ are, in principle, different. We expect R_s to be reduced with respect to the standard design due to the presence of the reflection killers. In this way, we can assume the whiskered focal line as a reflecting surface with a smaller reflectivity. So, the amount of signal that couples

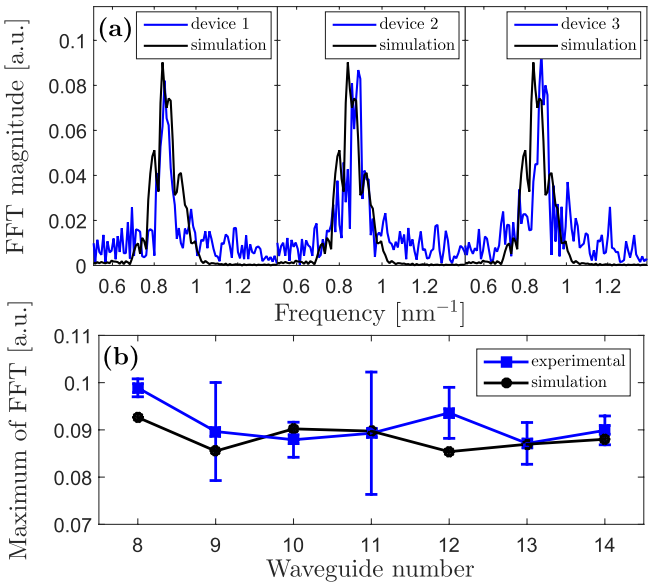

Fig. 4. (a) Comparison between the FFT of the simulated spectrum (black curves) and the FFT of three measured spectra (blue curves). The spectra refer to the 11-th output channel of three nominally identical devices. (b) Maximum value of the FFT at the FP frequency for experimental (blue) and simulated (black) spectra. The data are shown for the different output channels.

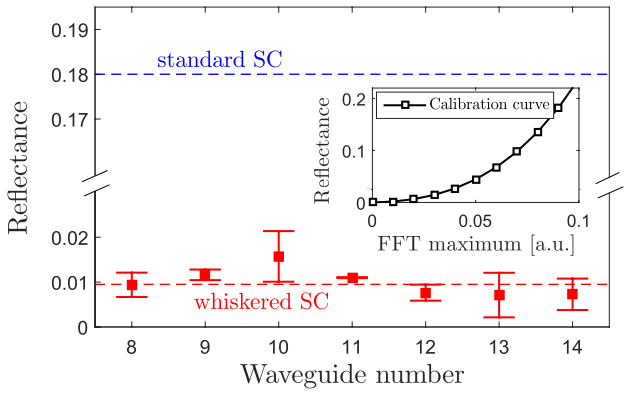

Fig. 5. In red the reflectance values experimentally obtained for the whiskered SC as a function of the different output waveguides. The dashed line represents the mean value. The blue dashed line represents the reflectance value for the standard SC design, as it comes from the FEM simulation. By using this reflectance value we calibrated the system, evaluating the best σ parameter appearing within (3) to be about 1.02. The calibration curve used to convert the maximum value of the FFT to a reflectance value is reported as inset.

into the adjacent waveguides is unmodified by the presence of whiskers and we can use the same σ value estimated for the standard SC.

From (3), we can simulate the transmission spectrum of each output waveguide, sweeping over the SC facet reflectance. For each reflectance we determine the corresponding maximum value of the FFT of the output signal. This allows us to build a calibration curve, which is shown as inset in Fig. 5. In this way we gain a tool that relates the maximum of the FFT performed on the experimental spectra to a SC reflectance value. The data obtained for the whiskered design are shown in Fig. 5, where they are compared with the simulated value of the standard SC reflectance.

By calculating the mean value, we find the reflectance of the whiskered SC being around $(9 \pm 1) \times 10^{-3}$. This result is definitely smaller than the one of the standard SC, about 0.18.

V. Conclusion

In this letter we achieved a suppression of the back-reflected light in the whiskered SC by more than one order of magnitude. Moreover, we developed a model, based on the scattering matrix theory, that well fits the experimental results. We emphasize that this approach is not addressed to reduce the reflection caused by narrow edges, that can be reduced using shallow etching, but allows for reducing the reflections from all the other surfaces of the SC. Our method can be a useful tool when special attention has to be paid to the interferential noise that affects the free propagation of beams. In particular, it can be exploited for increasing the performances of an AWG, that can be affected by the presence of unwanted internal reflections at the SC level.

References

[1] G. T. Reed and A. P. Knights, *Silicon Photonics: An Introduction*. Reading, MA, USA: Wiley, 2004.
[2] W. Bogaerts *et al.*, "Compact wavelength-selective functions in silicon-on-insulator photonic wires," *IEEE J. Sel. Topics Quantum Electron.*, vol. 12, no. 6, pp. 1394–1401, Nov./Dec. 2006.
[3] S. Pathak, M. Vanslembrouck, P. Dumon, D. Van Thourhout, and W. Bogaerts, "Optimized silicon AWG with flattened spectral response using an MMI aperture," *J. Lightw. Technol.*, vol. 31, no. 1, pp. 87–93, Jan. 1, 2013.
[4] J. Park, G. Kim, H. Park, J. Joo, S. Kim, and M.-J. Kwack, "Performance improvement in silicon arrayed waveguide grating by suppression of scattering near the boundary of a star coupler," *Appl. Opt.*, vol. 54, no. 17, pp. 5597–5602, Jun. 2015.
[5] J. Li, T.-R. Kim, H.-S. Kim, G.-Y. Oh, and Y.-W. Choi, "Lossy waveguide design considering polarization dependency to reduce back reflection in 2×1 MMI combiners," *Opt. Exp.*, vol. 22, no. 21, pp. 25953–25964, Oct. 2014.
[6] J. H. Schmid *et al.*, "Subwavelength grating structures in silicon-on-insulator waveguides," *Adv. Opt. Technol.*, vol. 2008, Jul. 2008, Art. no. 685489.
[7] Y. Gottesman, E. V. K. Rao, and B. Dagens, "A novel design proposal to minimize reflections in deep-ridge multimode interference couplers," *IEEE Photon. Technol. Lett.*, vol. 12, no. 12, pp. 1662–1664, Dec. 2000.
[8] S. J. McNab, N. Moll, and Y. A. Vlasov, "Ultra-low loss photonic integrated circuit with membrane-type photonic crystal waveguides," *Opt. Exp.*, vol. 11, no. 22, pp. 2927–2939, Nov. 2003.
[9] R. Takei *et al.*, "Silicon knife-edge taper waveguide for ultralow-loss spot-size converter fabricated by photolithography," *Appl. Phys. Lett.*, vol. 102, no. 10, p. 101108, 2013.
[10] P. D. Trinh, S. Yegnanarayanan, and B. Jalali, "5 × 9 integrated optical star coupler in silicon-on-insulator technology," *IEEE Photon. Technol. Lett.*, vol. 8, no. 6, pp. 794–796, Jun. 1996.
[11] G. B. Cao, L. J. Dai, Y. J. Wang, J. Jiang, H. Yang, and F. Zhang, "Compact integrated star coupler on silicon-on-insulator," *IEEE Photon. Technol. Lett.*, vol. 17, no. 12, pp. 2616–2618, Dec. 2005.
[12] A. Vonsovici and A. Koster, "Numerical simulation of a silicon-on-insulator waveguide structure for phase modulation at 1.3 μm," *J. Lightw. Technol.*, vol. 17, no. 1, pp. 129–135, Jan. 1999.
[13] S. Chen, Q. Yan, Q. Xu, Z. Fan, and J. Liu, "Optical waveguide propagation loss measurement using multiple reflections method," *Opt. Commun.*, vol. 256, nos. 1–3, pp. 68–72, Dec. 2005.
[14] B. E. Saleh and M. C. Teich, *Fundamentals of Photonics*, vol. 22. Reading, MA, USA: Wiley, 1991.
[15] W. S. C. Chang, *Principles of Lasers and Optics*. New York, NY, USA: Cambridge Univ. Press, 2005.